MULTIFREQUENCY ANALYSIS OF EDDY CURRENT DATA

D. Horn and R. Roiha
AECL, Chalk River, Ontario, Canada

Abstract: Modern multifrequency eddy current inspections typically produce more information than is actually processed by the analyst. The traditional "strip chart" and impedance-plane signal analysis presentations contain the data needed to simultaneously extract a number of quantities, including the depth profile and surface extent of flaws, the distance from the probe to the test piece, the character and amplitude of ferromagnetic signal components and the gap between conductive components. However, much of this information is hidden in correlations between the signals obtained at different frequencies. A simplified modeling algorithm, based on the same skin-depth considerations employed by industrial analysts, offers a relatively fast and quantitative solution to the "inverse problem" of deducing features from eddy current signals. The frequency response of the probe is approximated as a combination of effects, including conductor/flaw geometry, ferromagnetic response, and lift-off or fill-factor and the phenomena that combine to produce signals best approximating the observed response are displayed for consideration by the analyst. Real-world applicability of the techniques is illustrated by analysis of data from inspections of nuclear power plant components.

Introduction: Developments in eddy current probe technology and instrumentation have made it possible to collect far more data than present analysis techniques use. For example, the information contained in the correlations between signals obtained at different frequencies is seldom fully exploited. Extracting this information is a task well suited to computerization and, indeed, algorithms to reconstruct flaws from eddy current signals abound in the literature (see [1] for a review). Despite this, computerized analysis of industrial eddy current data is usually limited to having the computer facilitate the same process of amplitude and phase measurement that an analyst would have performed decades ago. This conservative approach may be partly because the more detailed calculations invert field modelling to obtain flaw geometry, which presents an enormous computing task; alternative methods include neural networks, which recognize patterns from training data, but fail to make use of electrodynamics and hence lack predictive capability. More generally, the great variety of defect types, material properties, contaminant signals, and conductor geometry make it difficult to program a computer to foresee all the eventualities that an experienced analyst would be able to interpret.

Our approach [2] does make quantitative use of physical principles, but simplifies the task to process indications in a reasonable time with the computing resources available to inspection teams. Analogous work with application to rotating coils is described in [3]. We calculate the effective signals due to each contributing feature from definite integrals of the simple frequency-dependent skin-depth expressions for phase and amplitude, and model the response of the probe as a vectorial combination of several effects. A regression minimizes the difference between the measured signal and the calculation at all frequencies by adjusting the features at each measured location. The phenomena that combine to produce signals best approximating the observed response are displayed for consideration by the analyst.

This paper provides a description of the underlying principles of our multifrequency analysis techniques and illustrates their applications with examples analyzing tube inspection data from simple bobbin-coil probes and sophisticated array probes.

Principles of Multifrequency Analysis: Our analysis exploits the known variation of eddy current signals with frequency. With multiple frequencies, several data may be obtained from a single location, permitting extraction of more than one property of the sample (e.g. distance to conductor, flaw depth, and support plate properties). The effective signals due to a trial set of conductor/flaw geometry and permeability parameters are calculated from definite integrals of the expressions for phase and amplitude, which explicitly contain a frequency dependence.

Calculation of a defect signal starts with the relationship of signal amplitude and phase to defect depth [4], valid for a small, nonconducting volume element interrupting the current flow at a given depth in the conductor. The net eddy current signal is the difference between the signal from the conductor with the nonconducting void and that from the unperturbed conductor. Its amplitude falls off exponentially with the depth of the defect and its phase is shifted by an amount which increases linearly with depth:

$$A(x,t) \propto e^{-2x/\delta} \cdot e^{i(\omega t - 2x/\delta)},$$

where x is the thickness of conductor between the probe and the nonconducting volume element and δ is the frequency-dependent skin-depth parameter. Amplitude does not exactly follow this skin-depth relationship for most geometries; however, we wish to find the approximate functional form of the signal behavior so that calibrated signals may be associated with physical quantities. For a macroscopic flaw, the expression should be weighted by the flaw surface area, S, normal to the x-direction, at each depth and integrated over its x-extent. The amplitude saturates as S exceeds the region of uniform field produced by the coil. See Figure 1 for a qualitative illustration of how the frequency dependence of the above expression may be exploited to obtain information about the depth profile of a flaw. When the entire surface area at a given depth sees approximately the same magnetic field, the expression for amplitude simplifies to

$$A \propto \int_{x_{\min}}^{x_{\max}} S(x) e^{-2x/\delta} dx,$$

where $x_{\min}$ and $x_{\max}$ are the minimum and maximum depth range of the void. Likewise, the amount by which the phase is reduced, $\Phi = 2x/\delta$, weighted by amplitude, can be integrated over the depth range of the void to obtain an average phase angle. This is an approximation; the phase and amplitude should ideally be obtained from a unified calculation, but this approach was retained for its simplicity and computational tractability. The phase integral becomes

$$\Phi = \frac{2}{\delta} \frac{\int_{x_{\min}}^{x_{\max}} x S(x) e^{-2x/\delta} dx}{\int_{x_{\min}}^{x_{\max}} S(x) e^{-2x/\delta} dx}.$$

Since eddy current instruments provide a relative phase measurement, which can be adjusted during analysis, the phase offset should be determined. It may be found by subtracting the calculation with limits $x_{min} = 0$ *mm* and x_{max} = *wall thickness* from the phases for through-hole calibration data for the frequencies used.

Other sample properties also provide signal components, which may be estimated analytically and added vectorially. For example the signal from nearby ferromagnetic materials, such as carbon steel support plates, can be reproduced by scaled trajectories in frequency space. Empirically, if flaw signals at all frequencies are normalized to a large-area far-surface wall loss, then ferromagnetic signal amplitudes decrease with increasing frequency. For consistency with the flaw calculations, we use a skin depth factor to introduce the frequency effect, in this case as approximately proportional to skin depth squared. A single quantity deduced from data analysis therefore reproduces amplitudes at all frequencies and is taken to represent presence of ferromagnetic support material. The corresponding phase values decrease with increasing

frequency; we take them as inversely proportional to skin depth. The phase-amplitude relationship is illustrated in Figure 2.

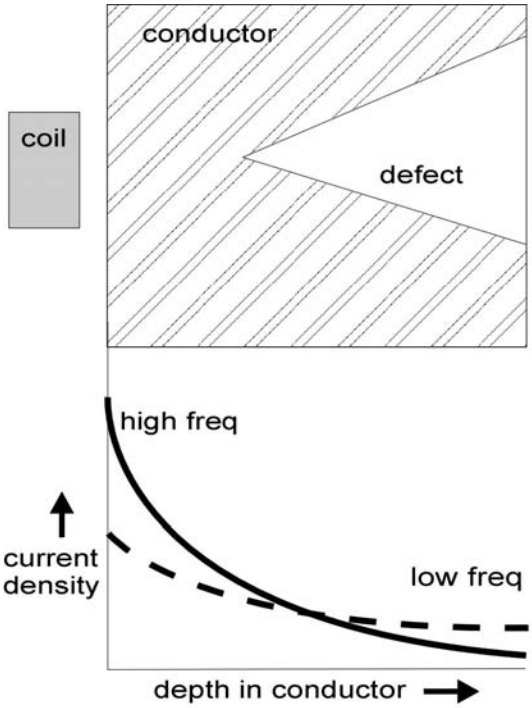

Figure 1: Schematic representation of eddy-current density as function of depth for high and low frequency. High frequencies are sensitive to the part of the defect nearest the coil and low frequencies are more sensitive to the total defect area at the far surface. Additional frequencies provide more information on the depth profile.

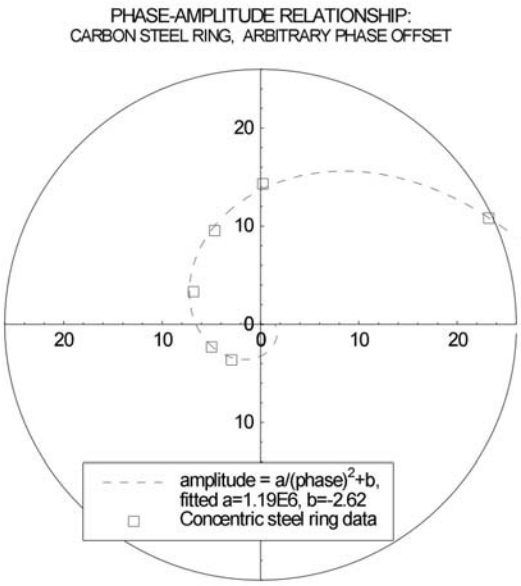

Figure 2: Polar plot of phase-amplitude relationship for eddy current signals from a concentric carbon steel ring Amplitude increases with decreasing frequency. Symbols are laboratory measurements at six frequencies (30, 70, 120, 240, 480, and 650 kHz); the dashed line is a fitted curve for amplitude linear in $(1/\text{phase})^2$.

Another effect is the distance from the coil to the conductor, which may manifest itself as lift-off or fill factor. The analytical expression for this will vary with coil configuration, but will again be frequency-dependent, with higher frequencies giving larger amplitudes that fall off more quickly with distance. A calibration factor, deduced from a known change in lift-off or fill factor, provides a distance scale for analyzed data. In parallel with the other signal computations, this calculation also uses the skin depth to introduce the frequency effects. Lift-off phase is generally rotated to zero. For impedance probes, the phase angle typically remains nearly constant over a large distance; for transmit-receive units, care must be taken to operate in a range where the angle does not change significantly.

Application to Tube Testing with Bobbin Probes: The general formalism outlined in the previous section may be applied to specific eddy-current testing objectives. Tube testing with an internal bobbin coil is a common technique for in-service steam generator inspection and multifrequency analysis is well suited to the quantitative interpretation of such results. The definite integrals of the flaw signal equations in the previous section are evaluated based on what is known about flaw morphology. For example, a specific flaw shape, such as that from pitting craters or from wear by flat components, may permit constraints to be put on the eddy current relationships. Somewhat more generally, volumetric defects, approximated as having a V-shaped

transverse cross section with depth and opening angle to be determined, lead to an expression for circumferential defect extent as a function of depth, $S(x) = S(\bar{x}) + m(x - \bar{x})$, with wall slope, m, and $\bar{x} = (x_{\min} + x_{\max})/2$. The consequent expressions for amplitude and phase are as follows:

$$A \propto \frac{\delta}{2}\left\{\begin{array}{l}\left[S(\bar{x}) - m\bar{x}\right]\cdot\left[e^{-2x_{\min}/\delta} - e^{-2x_{\max}/\delta}\right] + \ldots \\ m\cdot\left[(x_{\min} + \frac{\delta}{2})e^{-2x_{\min}/\delta} - (x_{\max} + \frac{\delta}{2})e^{-2x_{\max}/\delta}\right]\end{array}\right\},$$

and

$$\Phi = \frac{2}{\delta}\left\{\frac{(x_{\max}{}^2 - x_{\max}x_{\min} + \delta x_{\max} - \frac{\delta}{2}x_{\min} + \frac{\delta^2}{2})\cdot e^{-2x_{\max}/\delta} - (\frac{\delta}{2}x_{\min} + \frac{\delta^2}{2})\cdot e^{-2x_{\min}/\delta}}{(x_{\max} - x_{\min} + \frac{\delta}{2})\cdot e^{-2x_{\max}/\delta} - \frac{\delta}{2}\cdot e^{-2x_{\min}/\delta}}\right\}.$$

Signals due to ferromagnetic components are calculated as in the previous section, but with a phase offset depending on whether a circumferential conduction path is open or closed.

Lift-off amplitude, A_{lo}, may be calculated from the mean coil diameter, $\overline{D}$, and the change in fill-factor as defined in [1], from its nominal value, η_0, with the frequency dependence of the field spread introduced by the skin depth parameter, δ:

$$A_{lo} \propto \frac{\eta_0 - \eta}{(\overline{D} + a\delta)^2}.$$

In the specific example below, which treats a measurement of wear at support plates, the signal phases and amplitudes were calculated for each of four frequencies, based on the values of flaw depth, circumferential extent, tube support signal, and support phase offset. The values that give signals best reproducing the "strip chart" data of Figure 3a were tabulated as a function of axial position along the tube in part b of the figure. The fitted results for defect and support characteristics may be assessed in the table. A three-dimensional graphical depiction of tube wall features deduced from the above analysis is also possible, but data collected with bobbin coils contain no information about circumferential location, so some symmetries must be assumed in the reconstructed image. For example, the analysis may determine flaw circumferential extent as a function of depth, which is a major advance over earlier techniques, but would not distinguish between two different circumferential profiles having the same extent as a function of depth, nor would it distinguish between one defect and two separate smaller ones that sum to the same depth profile. With these limitations, the representation of Figure 3c permits visualization of the features. However, proper assignment of circumferential profile can only be achieved by analysis of data from a probe that resolves that dimension, *e.g.* a rotating probe or an array probe, as described in the next section.

Axial pos'n index	Wall (mm)	Circ. extent coeff.	FM ampli-tude	FM phase offset
1	1.10	0.08	0.00	64.98
2	1.10	0.08	0.00	64.98
3	1.10	0.08	0.00	64.98
4	1.10	0.08	0.00	64.98
5	1.09	0.08	0.44	65.00
6	1.10	0.08	0.00	64.98
7	1.10	0.08	0.00	64.98
8	1.10	0.08	0.00	64.98
9	1.10	0.08	0.00	64.98
10	1.10	0.08	0.00	64.98
11	1.10	0.08	0.00	64.98
12	1.10	0.08	0.00	64.98
13	1.10	0.08	0.00	64.98
14	1.10	0.08	0.00	64.98
15	1.10	0.08	0.00	64.98
16	1.10	0.08	0.00	64.98
17	1.10	0.08	0.00	64.98
18	1.10	0.08	0.00	64.98
19	1.10	0.08	0.00	64.98
20	1.10	0.08	0.00	64.98
21	1.10	0.08	0.00	64.98
22	0.98	0.08	0.51	65.84
23	0.93	0.21	1.19	79.23
24	0.74	0.09	1.38	68.20
25	0.73	0.10	1.76	63.69
26	0.66	0.10	1.78	66.59
27	0.57	0.10	2.05	70.02
28	0.72	0.15	1.86	71.41
29	0.72	0.14	1.84	72.80
30	0.97	0.33	1.42	71.88
31	0.95	0.23	1.24	71.45
32	0.91	0.08	0.63	66.35
33	1.10	0.08	0.00	64.98
34	1.10	0.08	0.00	64.98
35	1.10	0.08	0.00	64.98
36	1.10	0.08	0.00	64.98
37	1.10	0.08	0.00	64.98
38	1.10	0.08	0.00	64.98
39	1.10	0.08	0.00	64.98
40	1.10	0.08	0.00	64.98
41	1.10	0.08	0.00	64.98
42	1.10	0.08	0.00	64.98
43	1.10	0.08	0.00	64.98
44	1.10	0.08	0.00	64.98
45	1.10	0.08	0.00	64.98
46	1.10	0.08	0.00	64.98
47	1.10	0.08	0.00	64.98
48	1.10	0.08	0.00	64.98
49	1.10	0.08	0.00	64.98
50	1.10	0.08	0.00	64.98

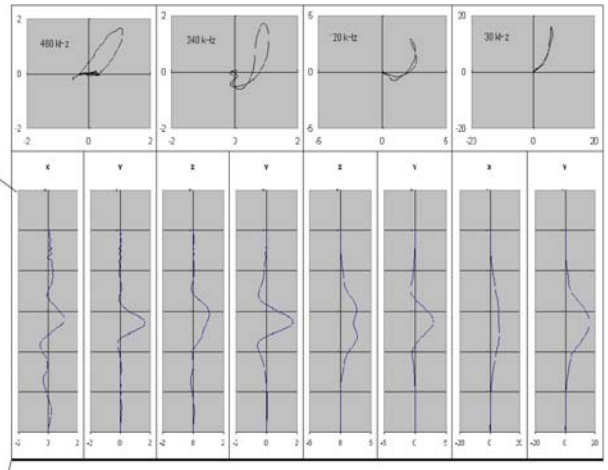

a) Four-frequency strip chart data

b) Deduced features

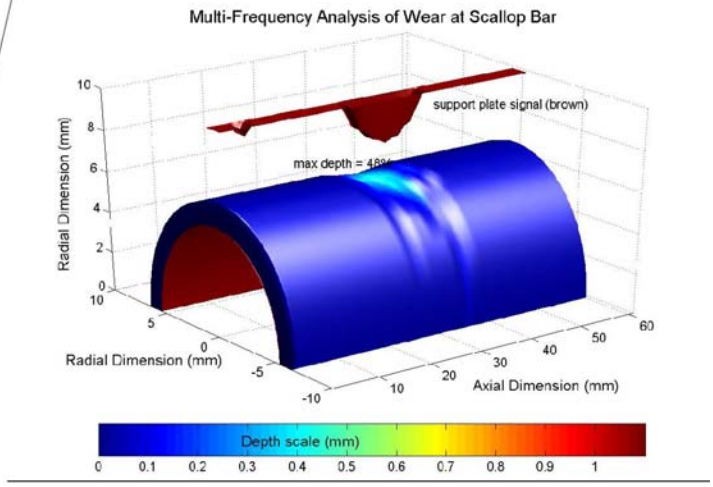

c) Graphical representation

Figure 3. Multifrequency analysis of "strip chart data" (graphed in panel a) to deduce features tabulated in panel (b) and visualized in panel (c).

Application to Tube Testing with Array Probes: The previous section notes that relative circumferential angle information may be obtained from analysis of rotating-probe or array-probe data. As an example, we discuss tubewall reconstruction based on X-probe measurements. The X-probe is an array probe with multiplexed transmit/receive units arranged to sample the complete circumference of the tube. The field distributions are different from those assumed for bobbin coils due both to the transmit/receive character of the probe and to the alignment of the coil axes normally to the tube wall. In analyzing X-probe data, more complex techniques are required, since both the amplitude of the signal and the spatial region over which it is observed must be considered separately for axially and circumferentially oriented transmit/receive units,

and the two orientations combine to produce a physical representation of the feature within the tube wall. One aspect of analysis is simpler, in that circumferential depth profiles are obtained from the angular distribution of the array elements; this frees the information contained in the frequency dependence of amplitude for use in extraction of other parameters. Figure 4 shows an axial tubewall profile generated from a single circumferential location around or on a calibration tube that was scanned simultaneously by one axially and one circumferentially oriented transmit/receive unit. The tube contains a simulated tubesheet expansion under a carbon steel ring that simulates the tubesheet material. It also has narrow and wide circumferentially oriented grooves and a 40%-through-wall flat-bottomed hole. The features are well reproduced by the results of the analysis. Spatial deconvolution of the eddy current signal as the probe scans axially has been discussed elsewhere[2]. This provides a positional response that is sharper than otherwise permitted by the field spread of the probe. Note that the concentric grooves have a larger circumferential component than the flat-bottomed hole, as indicated by the positive-going lobes of the orientation curve.

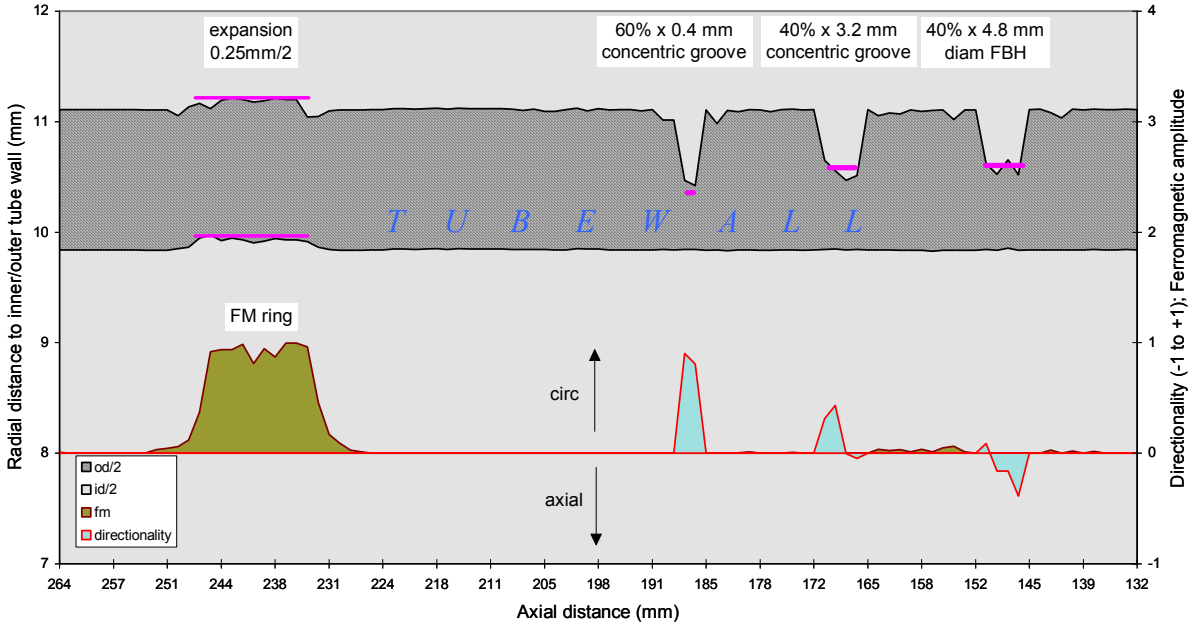

Figure 4. Multifrequency analysis of calibration tube data with five variables fitted simultaneously: ferromagnetic amplitude, lift-off, wall loss, and circumferential and axial extents. Heavy horizontal lines indicate the actual depths and extent. Left-hand axis shows radial distance to inner wall of tube (from lift-off) and to outer wall (inner plus calculated remaining wall). Right-hand axis indicates ferromagnetic amplitude from steel ring and relative amount of circumferential and axial component in tube feature.

The single set of coils processed in the above example cover a single circumferential location. As the full complement of X-probe coils are incorporated, reconstruction of the entire tubewall becomes possible and detailed profiling of artificially produced axial cracks in steam generator tubing is performed[2] giving a root-mean-square error of 8% over 80 sampling locations. Tubewall reconstruction with a different version of the probe and a different test piece was reported recently[5]. The work is part of a project to develop analysis software that will pre-process, calibrate, and analyze in-service inspection results for steam generators in nuclear power

plants. The top portion of Figure 5 shows a three-dimensional representation of analysis results for a tube segment with familiar calibration features. The plot is semitransparent so internal diameter and external features may be viewed simultaneously. A photograph of the segment is shown for comparison in the lower part of the figure. Based on the running time for analysis of the sample, we estimate that a 50-mm-long region of interest, e.g. at the tubesheet transition, could be processed in about ten minutes with the present generation of analysis computers.

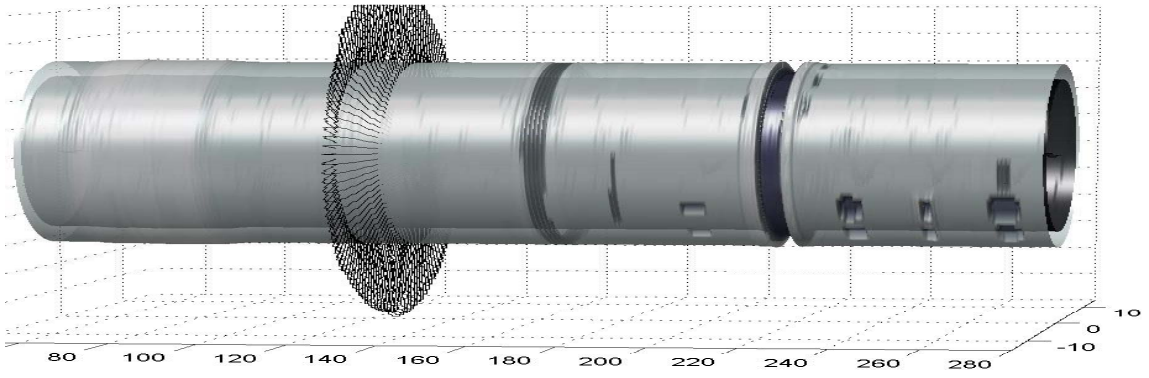

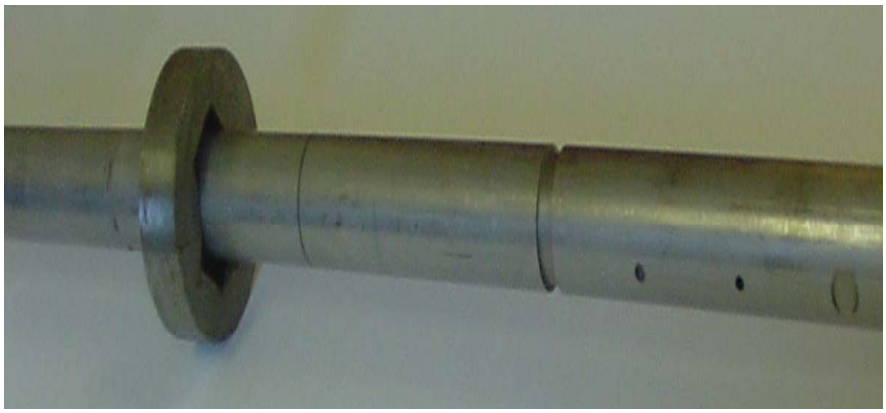

Figure 5: Multifrequency analysis results (top) showing expansion, steel ring signal, and EDM calibration features. Photograph of calibration tube (bottom).

Conclusions: Quantitative analysis of the correlations between eddy-current signals acquired at multiple frequencies can provide a breakdown of the contributions from various phenomena to the overall probe response. Multifrequency analysis separates the effects of the flaw depth profile, nearby ferromagnetic objects, and distance to the conductor surface, permitting assessment of each. Applied to tube inspection by bobbin coils, the method described provides more information than traditional multifrequency mixing. For array probe analysis the technique offers the potential for computerized analysis leading to three-dimensional tubewall reconstruction. Software for analysis of data from industrial inspection of nuclear power plant steam generator tubing is under development.

References:

[1] Auld, B.A. and Moulder, J.C., "Review of Advances in Quantitative Eddy Current Nondestructive Evaluation", J. Nondestr. Eval. 18 (1999)3.

[2] Horn, D., "Computer-assisted Multi-frequency Analysis of Array Probe Data", Proceedings of the 4th CNS International Steam Generator Conference. Toronto (May 2002).

[3] Bakhtiari, S. et al., Computer-Aided Analysis of Eddy Current Rotating Probe Data, Proceedings of the 4th CNS International Steam Generator Conference. Toronto (May 2002).

[4] Cecco, V.S., Van Drunen, G. and Sharp, F.L., Eddy Current Manual, Volume 1, AECL Report AECL-7523 (Rev. 1), 1981 November.

[5] Horn, D., Roiha, R. and Lu, J. "Advances in Analysis of Eddy-Current Data from Steam Generator Inspections", Proceedings of the Sixth CNS International Conference on CANDU Maintenance, Toronto, (November 2003).